INTERNATIONAL JOURNAL OF
COASTAL, OFFSHORE & ENVIRONMENTAL ENGINEERING IJCOE Vol.11/No. 1/Winter 2026 (81-90)

Available online at: www. ijcoe.org

Investigation the impact of wave charactristics and PTO parameters on the performance of a Two-Body Floating Point Absorber in the Gulf of Oman

Saeed Najafi
Assistant Professor, Iranian National Institute for Oceanography and Atmospheric Science (INIOAS);
s.najafi@inio.ac.ir

ARTICLE INFO

Article History:
Received :31 Aug 2025
Accepted :02 Feb 2026

Keywords:
Self-Reacting Floating-Point Absorbers
Wave energy converters
CFD
Power take-off
Gulf of Oman

ABSTRACT

The present research studies the impact of wave charactristics as well as the power take-off (PTO) damping on the hydrodynamic performance of a two-body floating point absorber (FPA) which sometimes called self-reacting point absorber (SRPA) or two-body wave energy converter (WEC) device. This type of WEC is designed for operation in the Gulf of Oman and its geometry is inspired from the famous reference model (RM3) which was developed at the National Renewable Energy Laboratory (NREL), United States. The numerical model was developed in the Siemens STAR-CCM+ software which solves the complete form of fluid governing equations. The parameters of the incident waves, was selected based on the previous researches on this region and PTO damping is specified based on the RM3 model design. The results show that changes in wave period and PTO damping significantly influence energy capture and converter efficiency. The results show that the absorbed power increases monotonically with wave height and reaches a maximum at a wave period of 6 s, indicating a clear resonant response of the two-body WEC across all tested sea states.

1. Introduction

Ocean waves represent one of the most persistent and underutilized renewable energy resources available to coastal regions (Chen et al., 2023; Evans, 1981; Falnes, 2007; Ishaq et al., 2023; Li & Yu, 2012). Their high energy density, predictability over daily and seasonal cycles, and global abundance make wave energy conversion an attractive complement to more variable sources such as wind and solar. Over the past several decades, a broad range of Wave Energy Converters (WECs) has been proposed, each attempting to harvest the oscillatory motion of waves through buoyancy-driven mechanisms, hydrodynamic forces, or pressure variations below the free surface. Among these technologies, the point absorber concept has emerged as one of the most versatile designs due to its compact footprint and ability to extract energy from multiple wave directions (Liu et al., 2022; Soleimani et al., 2023).

Early point absorber systems consisted primarily of a single buoy oscillating relative to a fixed seabed-mounted structure. Foundational studies in the 1970s established the theoretical basis for these devices, revealing how their hydrodynamic behavior and resonant response could be exploited to maximize absorbed power (Salter, 1974; Budar & Falnes, 1975). However, single-body point absorbers face inherent challenges in environments where tidal fluctuations significantly alter the effective distance between the free surface and the seabed (Evans, 1976; Mei, 1976; Newman, 1976). These variations can degrade the system's mechanical leverage and ultimately reduce its energy capture potential (Ma et al., 2020).

To address these limitations, researchers later introduced multi-body concepts in which a floating element interacts with a secondary reactive body rather than a rigid seabed. Two-body Floating Point Absorbers (FPAs) allow the device to harvest energy from the relative heave motion between the two bodies, making them largely insensitive to water-level changes (Beatty et al., 2015; Liang & Zuo, 2017; Yu & Li, 2013). This configuration has since become a cornerstone of modern WEC development, with experimental and numerical studies demonstrating its superior energy extraction efficiency under a wide range of sea states. Several prototypes—including multi-float systems and hybrid configurations—have further expanded the design space, highlighting the

broader potential of multi-body devices within the renewable marine energy sector (OPT, 2023).

Moreover, FPAs with three or more bodies have been proposed. (Rhinefrank et al., 2010) created a model scale with a control system, demonstrated through wave tank tests, which later led to the formation of Columbia Power Technology. (Stansby et al., 2017) developed the WEC M4, a moored three-float line absorber, to enhance power capture through experimental methods. (Sricharan & Chandrasekaran, 2021) introduced an innovative floating WEC with multiple floating bodies and a hydraulic PTO system. This device features a central buoy connected to surrounding floating bodies via a lever arm and is stabilized using a taut-mooring system.

(Falnes, 1999) conducted a theoretical study on a two-body FPA device, demonstrating that the relative heave motion between two axisymmetric bodies can absorb wave power. He showed that it is feasible to capture all the power in an incident wave with a crest length equal to the wavelength divided by 2π. He provided a theoretical proof of maximum power without detailed analysis. This study aims to offer a comprehensive theoretical analysis of a two-body system.

(Li & Yu, 2012) demonstrated the maximum power output of a two-body FPA with limited parameters. (Windt et al., 2021) explored maximum power at different scales using the Reynolds-averaged Navier–Stokes equation, while (Zheng et al., 2021) examined the scaling effect through experimental tests, smooth physical hydrodynamics, and theoretical analysis. These studies highlighted the benefits of multiple-body FPAs over single-body FPAs. However, the impact of various factors on the power output of multiple-body FPAs remains unclear, which is crucial due to the high costs of the tools used.

Our research focuses on the computational fluid dynamics (CFD) analysis of a two-body floating point absorber to optimize its performance under different wave and PTO parameters. This device was intended to work under the environmental conditions of the Gulf of Oman. The Gulf of Oman, a semi-enclosed sea with moderate but reliable seasonal wave activity, provides a unique case for exploring such design sensitivities. Although the region's wave power potential is lower than that of open-ocean sites, the area remains attractive for small- and medium-scale WEC deployment due to its proximity to coastal infrastructure and the seasonal consistency of wave patterns. Prior studies have characterized the local wave climate, identifying periods during the summer monsoon season in which wave heights and dominant periods align with the operational range of many point absorber concepts.

The PTO system is vital for converting mechanical energy from the wave-induced motion of the FPA into electrical energy. It typically includes components such as hydraulic rams, electrical generators, or mechanical systems tuned to the device's motion. Key factors influencing power performance is PTO damping, which control the device's response to wave forces. Improper tuning of this parameter can result in inefficient energy capture or even structural failure. By varying PTO parameters, the optimal conditions that maximize energy absorption and converter efficiency was identified. The findings of this research could lead to more efficient designs of FPAs and contribute to the advancement of wave energy technology.

2. Methods and Materials

2.1. Site Selection

Based on previous studies on the wave energy assessments, northern coasts of the Gulf of Oman, near the coast of Chabahar exhibit strong wave energy, specially from June to September. Based on the field measurements, significant wave height varies between 0.5 and 2 meters while peak period changes from 4 to 10 seconds (Saket et al, 2012). As shown in the **Figure 1**, they investigated four regions with highest annual mean power. Some major parameters including location, depth of water, distance to mainland and mean wave power are listed in **Table 1**. Based on the two last columns of Table, the present research focused on site B because it has minimum distance to the coastline and highest value of mean annual wave power which is 2.82 (kW/m).

Table 1: Main characteristics of selected areas in north part of the Gulf of Oman

Station ID	Lat. ºN	Long. ºE	Depth (m)	Distance to coastline (km)	J_{mean} (kW/m)
A	25.28	59.27	38.2	17	2.7
B	25.32	59.87	41	4.5	2.82
C	25.28	60.14	40.9	7	2.78
D	25.22	60.47	38	7.5	2.72

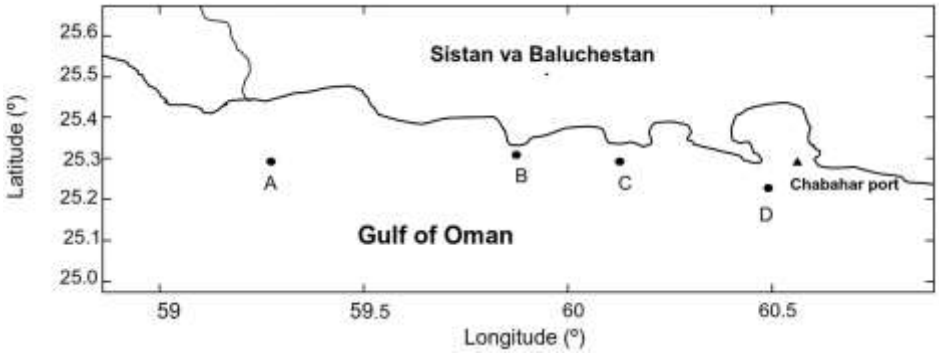

Figure 1: The selected locations for study of FPA performance

Based on the water depth in this region which is approximately 70 meters, a conceptual sketch of a two-body FPA with appropriate dimensions which is inspired from the famous reference model (RM3) and is shown in Figure 2. The performance of the FPA device was modeled using computational fluid dynamics (CFD) simulations to capture the complex interactions between the waves, the floating structure, and the power take-off (PTO) system. The numerical approach used in this study involves simulating the fluid-structure interaction (FSI) between the water waves and the floating device, taking into account the effects of significant wave height and different wave periods.

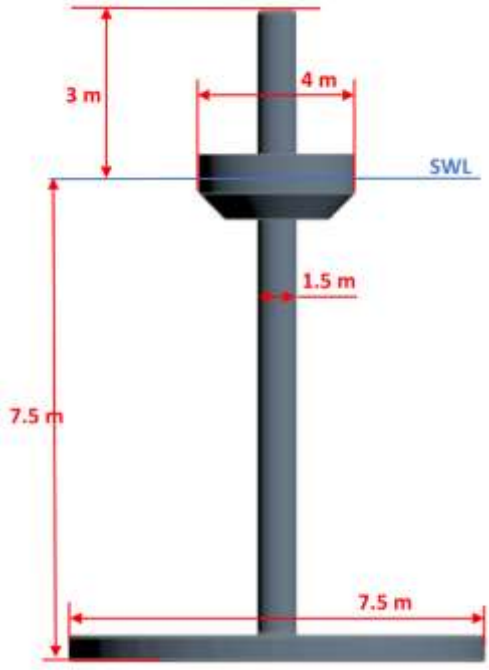

Figure 2: FPA model with main dimensions

2.2. Numerical Model Setup

A comprehensive hydrodynamic model was developed using Siemens STAR-CCM+, a multiphysics simulation platform capable of resolving the nonlinear free-surface behavior and fluid–structure coupling inherent to wave energy systems. The model employs an Unsteady Reynolds-Averaged Navier–Stokes (URANS) formulation, augmented with a Volume of Fluid (VOF) method to represent multiphase interfaces and wave deformation with high fidelity. The model consists of two main parts: the hydrodynamic model for simulating wave propagation and the mechanical model for the FPA's response to wave forces. The two-body FPA was modeled with precise geometric specifications, including dimensions, mass properties, and hydrodynamic coefficients. The two bodies consist of a primary floating body and a secondary submerged body, connected by a power take-off (PTO) system with adjustable damping coefficient. The main charactristic of the WEC for prototype and subscale of RM3 are summurized in the table below.

Table 2: Main particulars of the RM3 WEC for full-scale and 1:4 sub-scale

Parameter	Full Scale	1:4 Model
Float diameter (m)	20	5
Float draft (m)	3	0.75
Spar diameter (m)	6	1.5
Plate diameter (m)	30	7.5
Total draft (spar+plate) (m)	30	7.5
Float mass (kg)	727000	11360
Spar+plate mass (kg)	912800	14260
Heave natural period (s)	9	4.5
Heave natural frequency (rad/s)	0.698	1.4
Hydrostatic stiffness, K (kN/m)	270	17
Opt. PTO Damping (kN.s/m)	7000	225
Design Wave height, H (m)	3	0.75
Design Wave period, T (s)	12	6

The fluid domain represents the ocean environment and the waves acting on the FPA. To simulate the dynamic behavior of the WEC, an unsteady Reynolds-averaged Navier–Stokes (URANS) model was employed with a $k-\epsilon$ turbulence model on a finite-volume grid. For temporal discretization, a second order scheme was employed. To track the free surface deformations of the multiphase flow, a volume of fluid (VOF) model was used. The governing equations are as follows:

$$\frac{\partial \boldsymbol{u}}{\partial t} + (\boldsymbol{u}.\nabla)\boldsymbol{u} = -\frac{1}{\rho}\nabla p + \nu\nabla^2\boldsymbol{u} + \boldsymbol{f} \quad (1)$$

$$\nabla.\boldsymbol{u} = 0 \quad (2)$$

where:

- $\boldsymbol{u}$ is velocity field,
- p is the pressure,
- ν is the kinematic viscosity,
- ρ is the fluid density,

$\boldsymbol{f}$ represents the external forces including gravity and wave forcing.

Wave conditions was generated using a fifth-order Stokes wave formulation, providing a robust representation of nonlinear wave kinematics. These synthesized waves were introduced through a motion-specified boundary condition that enforces the desired free-surface profile and fluid particle velocity near the inlet. Figure 3 shows a schematic of device as modeled in the software. Only heaving motion was considered in this research, thus both the floating and reactive parts were allowed just one degree of freedom in vertical (z) direction and the wave propagation is aligned in the horizontal (x) direction. The more details about the computational model such as boundary conditions, domain particulars, wave damping near the outlet boundary and motion dynamics are presented in the subsequent subsections.

2.3. Computational domain

A schematic view of the computational domain for simulations of the two-body FPA device is shown in Figure 3. The three boundaries at left, front and back are set to Velocity inlets, in which the fluid velocity components and volume fraction are preset. Bottom boundary represent a no-slip wall. To consider the real flow effects, no symmetry planes were defined and numerical model was defined three dimensional. A pressure outlet boundary, where the condition of hydrostatic pressure of water column and volume fraction of light and heavy fluid is specified at the right and top side of the domain. Moreover, to avoid the water entry from the outlet boundary into the domain, a numerical damping region is defined at right side of the domain with prescribed coefficients based on software recommendations. The FPA body surface was considered as no-slip wall as well.

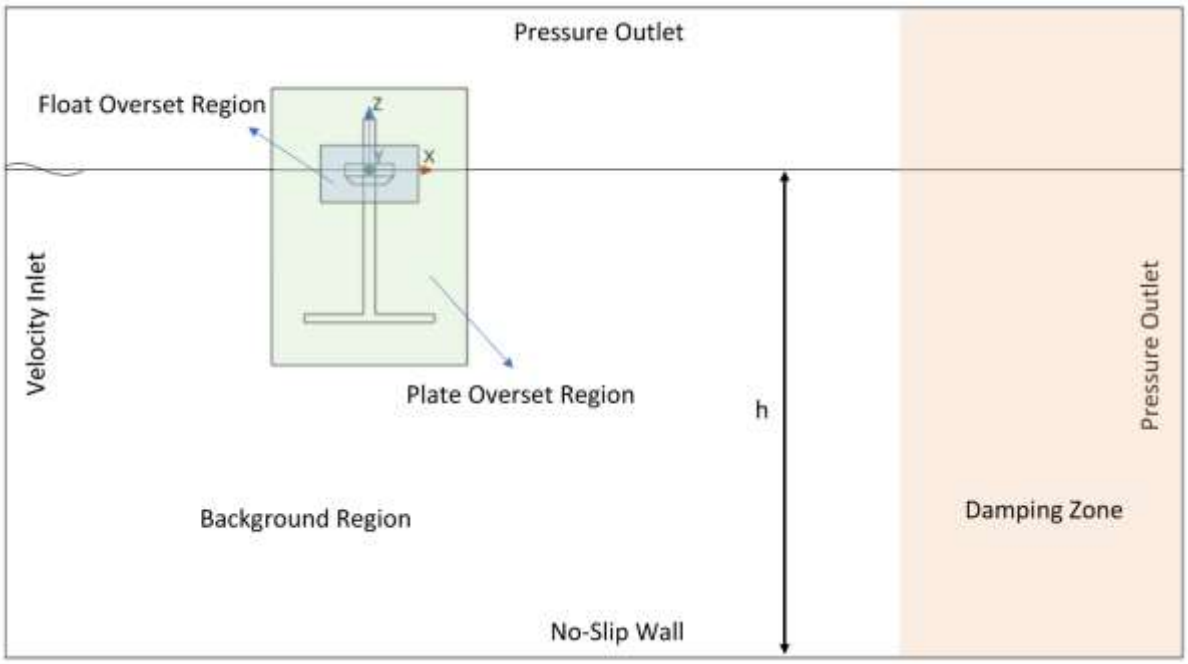

Figure 3: Domain particulars and overset grids used for FPA

The computational domain consists of three separate mesh zones. One background mesh which represent the fluid basin and two overset mesh which encompass the floating and reactive parts of the WEC. Overset grids were created using the unstructured polyhedral grids and can move over the background mesh which was created using the structured hexahedral grids. To increase the accuracy of the results, a set of refinement zones were defined in the regions with high gradients of the flow parameters.

Table 3: Characteristics of the numerical model

Wave Parameters		
Wave Period	4~10	s
Wave Height	0.4~2.0	m
PTO Parameters		
Damping Constant	50~350	$kN.s/m$
Domain Geometry		
Domain length	300	m
Domain height	100	m
Domain width	100	m
Water depth	70	m

Height of Free Surface Zone	3	m
Length of Damping Zone	80	m
Solver Parameters		
Time Step	0.05	s
Total Physical Time	100	s
Mesh Parameters		
Total Number of Cells	2257180	–
Number of Cell in Background	2020342	–
Cells in Floating Overset	75724	–
Cells in Reactive Overset	111114	–

The time step for the transient simulations was chosen to maintain Courant–Friedrichs–Lewy (CFL) numbers well below unity, ensuring numerical stability and capturing rapid changes in free-surface shape (Courant et al., 1928). The time discretization was performed using a second-order accurate scheme to preserve phase fidelity in the oscillatory motion of the device.

$$CFL = \frac{u\,\Delta t}{\Delta x} \quad (3)$$

The CFL number defines the number of cells which the fluid particles can travel through in each time step. Regarding in a free surface flow, the characteristic velocity represented by phase velocity of the wave ($v_p = \lambda/T$), and the number of cells in x direction in a wave length is ($n = \lambda/\Delta x$), we may have:

$$CFL = \frac{\lambda \Delta t}{T \Delta x} \rightarrow \Delta t = \frac{CFL.T}{n} \quad (4)$$

Thus, to preserve the CFL in a stable range, time step could be estimated for each test case. To capture the boundary layer near the body surface, prismatic layer meshes created around the floating and reactive parts. The cell size at the first layer is set such that the y^+ in the wall function is about ($y^+ \approx 150$). Figure 4 shows a cross section of the boundary layer cells around the reactive part as well as the numerical grid around floating point wave energy converter. To determine the optimum mesh size, a gris study was carried out and final model includes more than 2,250,000 computational prismatic cells in total. Simulation time was considered 100 s in all cases with time step of 0.05 seconds.

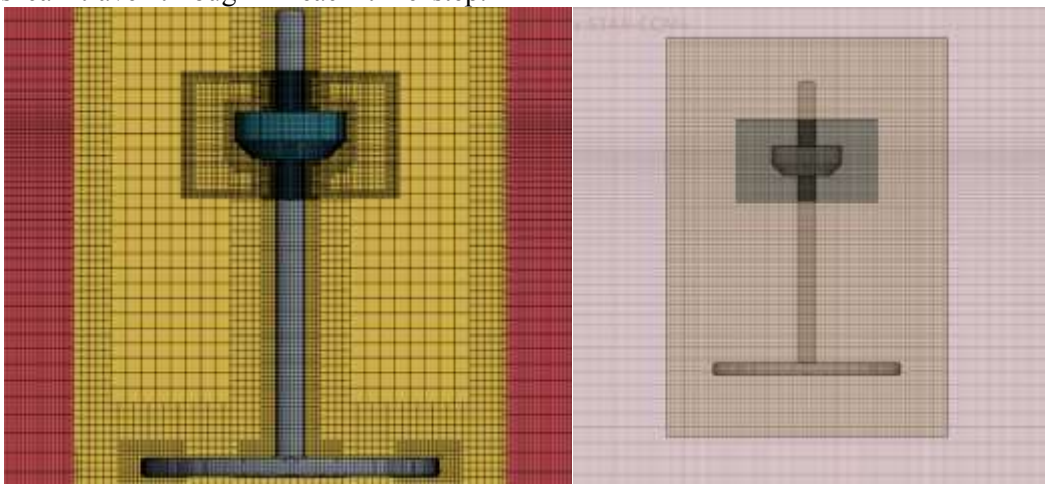

Figure 4: Numerical grid around wave energy converter

2.4. Damping zone

One of the most crucial issues in modeling the numerical wave tanks is treatment of the backflows and wave reflections from the boundaries. Since in the water waves problem, the fluid particle trajectory is orbital, a simple pressure outlet boundary cannot handle this issue. To alleviate the problem, a damping zone usually defined on the pressure outlet boundaries (Figure 3). The length of damping zone is defined two times of the wave length as Star-CCM+ guidelines. In the damping zones, the velocity components are mitigated using a resistant term which increases quadratically with distance towards the outlet boundaries and ideally, the wave amplitude vanishes as they approach to the outlet boundaries (Choi & Yoon, 2009). In some references, it is called the numerical beaches.

2.5. Power take-off (PTO) system

To harvest the energy from two-body FPA, a PTO mechanism must be implemented between floating and reactive parts. In the most cases, a spring-damper system used to take out power from the system. Normally, due to inherent hydrostatic stiffness of the buoy, PTO stiffness is ignored and the only effective PTO parameter is damping of power take-off system which controls the dissipation of energy. For each simulation, the PTO damping is varied across a predefined range to assess its impact on the overall performance of the FPA. As mentioned in the **Table 2**, in this study, damping varies from 150 to 400 $kN.s/m$. This range is selected based on prior wave tank experiments on RM3 (Xu et al., 2023). Generally, the PTO force is proportional to the relative position and the velocity of the bodies. One can write:

$$z = z_f - z_r \quad (5)$$

In which z_f and z_r represent the vertical position of floating and reactive parts respectively. The damping component of the PTO mechanism can be expressed with constant b_{PTO} and is related to the relative velocity of two bodies as:

$$F_{damping} = -b_{PTO}\dot{z} \quad (6)$$

Where $\dot{z}$ is relative velocity between two components. Time-averaged absorbed power by the PTO mechanism is defined by:

$$P = \frac{1}{2} b_{PTO}|\dot{z}|^2 = \frac{1}{2} b_{PTO}\omega^2|z|^2 \quad (7)$$

3. Results and Discussion

This section presents the hydrodynamic response of the two-body floating point absorber (FPA) under different PTO configurations and wave conditions. All simulations were carried out after ensuring numerical stability and convergence of the CFD model.

3.1. Model Validation with Heave Decay

Before evaluating the effect of wave and PTO, the numerical model was validated against experimental heave decay measurements. In this step, the floating and reactive bodies were rigidly connected, converting the system into an equivalent single-degree-of-freedom heaving cylinder. Figure 5 demonstrates excellent agreement between the numerical and experimental time response of heave oscillations. The good agreement between numerical and experimental measurments confirms that the CFD model accurately captures both radiation and diffraction effects, enabling reliable assessment of PTO-coupled motions.

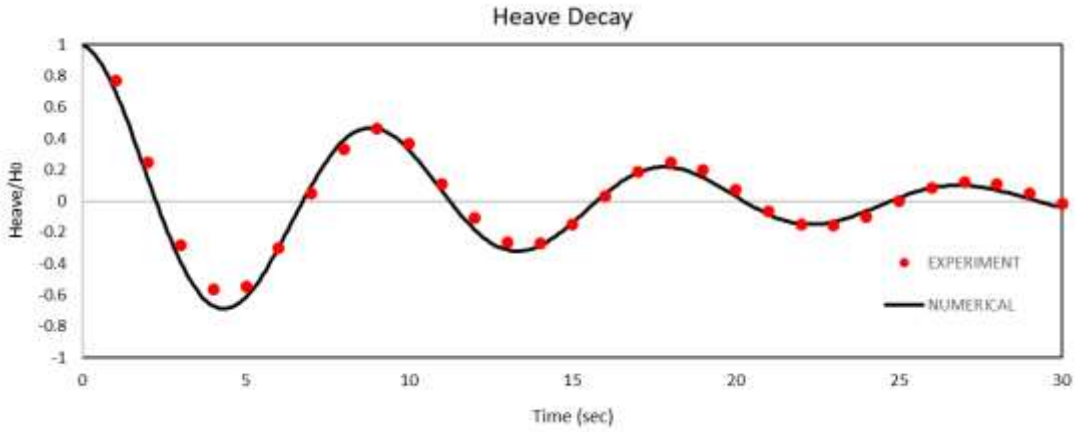

Figure 5: Comparison between experimental and numerical results of heave decay test

3.2. The effect of PTO Stiffness

PTO damping is a key parameter governing energy extraction, as it dictates the rate at which mechanical motion is converted into useful power. To quantify its impact, damping values ranging from 50 to 350 kNs/m were examined across wave periods from 4 to 10 seconds.

Figure 6 shows the absorbed power as a function of wave period for different damping levels and a clear bell-shaped pattern appears in each case. These findings support the results of (Li & Yu, 2012), who reported a similar bell-shaped trend between damping and energy capture. As seen in the figure, at low damping, because the system undergoes large oscillations, the force applied by the PTO is large enough to extract significant power. However, as expected this trend reversed with increasing the wave period due to changing the frequecy of excitation force.

At the moderate dampings (200-300 kNs/m), the energy absorption in a large interval of periods, has no significant changes and almost remains uniform. At high damping, the device becomes overdamped, suppressing relative motion between bodies and abrosbed power reduced.

Because dominant wave period of the region is between 6 to 7 seconds, the optimum damping would be around 100 kNs/m, which coincides closely with the device's natural period. This behavior is consistent with classical hydrodynamic theory, in which maximum power extraction occurs when mechanical damping equals radiation damping.

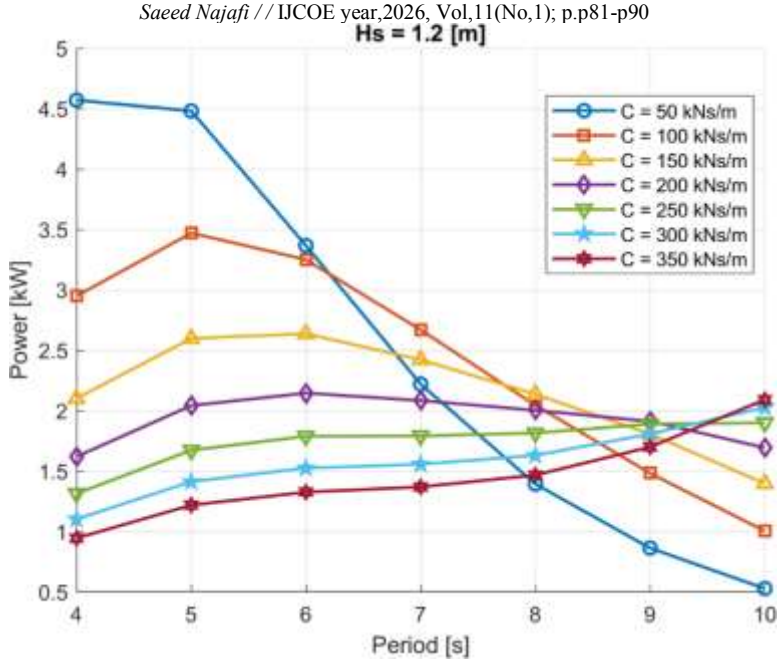

Figure 6: Absorbed power in different PTO damping in Hs=1.2 m

3.3. The effect of environmental conditions

Following the absorbed power of WEC is plotted in different wave conditions for different damping values of PTO. These types of curved is known as power matrix which extensively used for calculation of annual energy production (AEP) of wave energy devices in conjunction with joint probability distribution (JPD) of sea states.

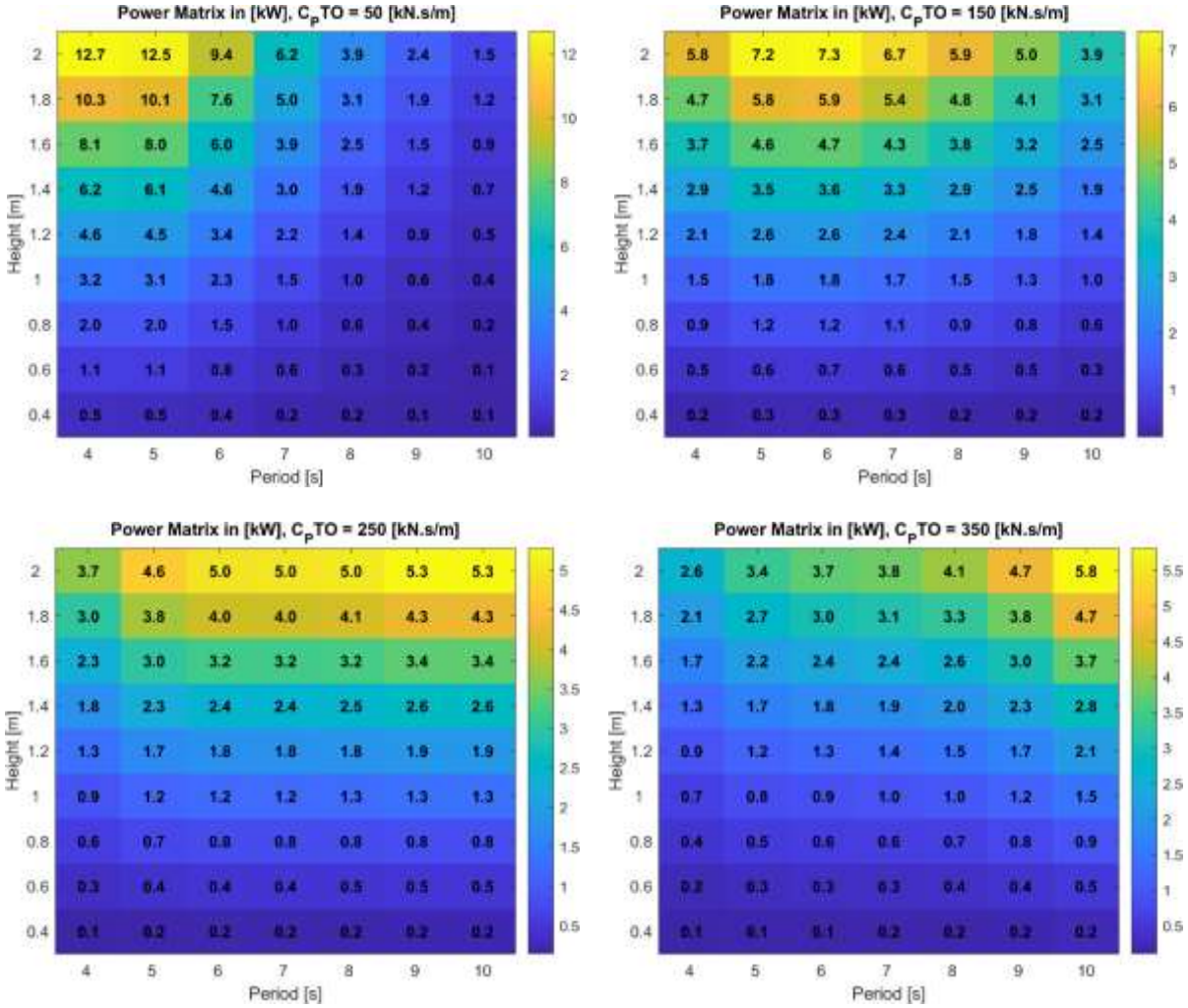

Figure 7: Power matrix of WEC in different sea states and dampings

Based on the absorbed power data presented in the each contour plots, several key trends emerge. First, absorbed power increases consistently with wave height across all periods, which is expected since wave energy flux is proportional to the square of wave height. For the largest wave height considered (2.0 m), the maximum absorbed power reaches approximately 12.7 kW at a wave period of 4 s, while the smallest wave height (0.4 m) yields negligible power (<0.2 kW) regardless of period. This monotonic relationship highlights the strong sensitivity of the two-body WEC to incident wave amplitude, emphasizing the importance of siting in energetic sea states.

The plot also reveals a clear resonant behaviour with respect to wave period. For all wave heights above 0.8 m, the absorbed power peaks at a period of near 6 seconds, with secondary peaks or plateaus at 5 s and 7 s. For instance, when PTO damping set around 200 kNs/m, at H = 2.0 m, power at T = 6 s is about 6.0 kW, compared to 5.7 kW at 5 s and 5.8 kW at 7 s, indicating a relatively broad, near-symmetric response around the natural period of the device. As wave height decreases, the peak becomes less pronounced but remains centred at 6 s. This suggests that the optimal PTO damping selected for this test case is well-tuned to the primary resonance of the two-body system, yielding consistent energy capture over a range of operational conditions.

From a design perspective, the relatively flat response between 5 and 7 s for moderate to high wave heights (e.g., H ≥ 1.2 m) is advantageous, as it implies the device can maintain satisfactory performance even when the sea state deviates from the exact resonance period. However, for very small wave heights (H ≤ 0.6 m), absorbed power becomes uniformly low across all periods, indicating a practical threshold below which energy extraction is not economically viable. These results underscore the need for adaptive PTO control strategies to broaden the effective bandwidth and improve low-height performance, while also confirming that the current design is well-suited for sites with characteristic periods around 6 s and significant wave heights above 1 m.

3.4. Free surface profile

Time history of buoy motions in seven periods as well as the snapshots of the device's relative motion over a full wave cycle is illustrated in the following figures. A clear interplay among incident, radiated, and diffracted wave components is shown in the plots.

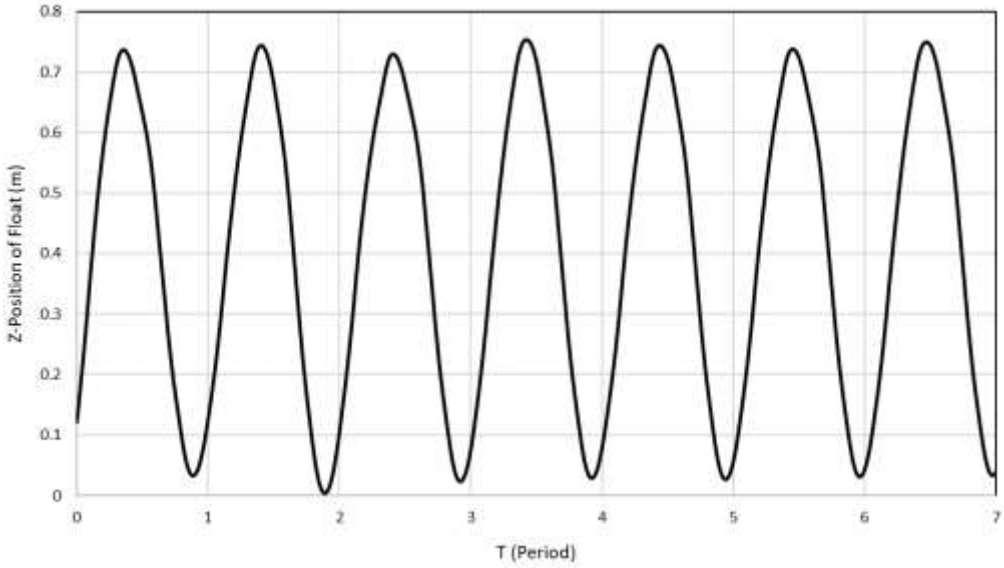

Figure 8: Time history of the floating part heave motions

The free-surface elevation plot at four time stamps reveals radiated waves propagating outward from the reactive body. These waves are a physical manifestation of radiation damping, a hydrodynamic mechanism essential for effective wave energy extraction.

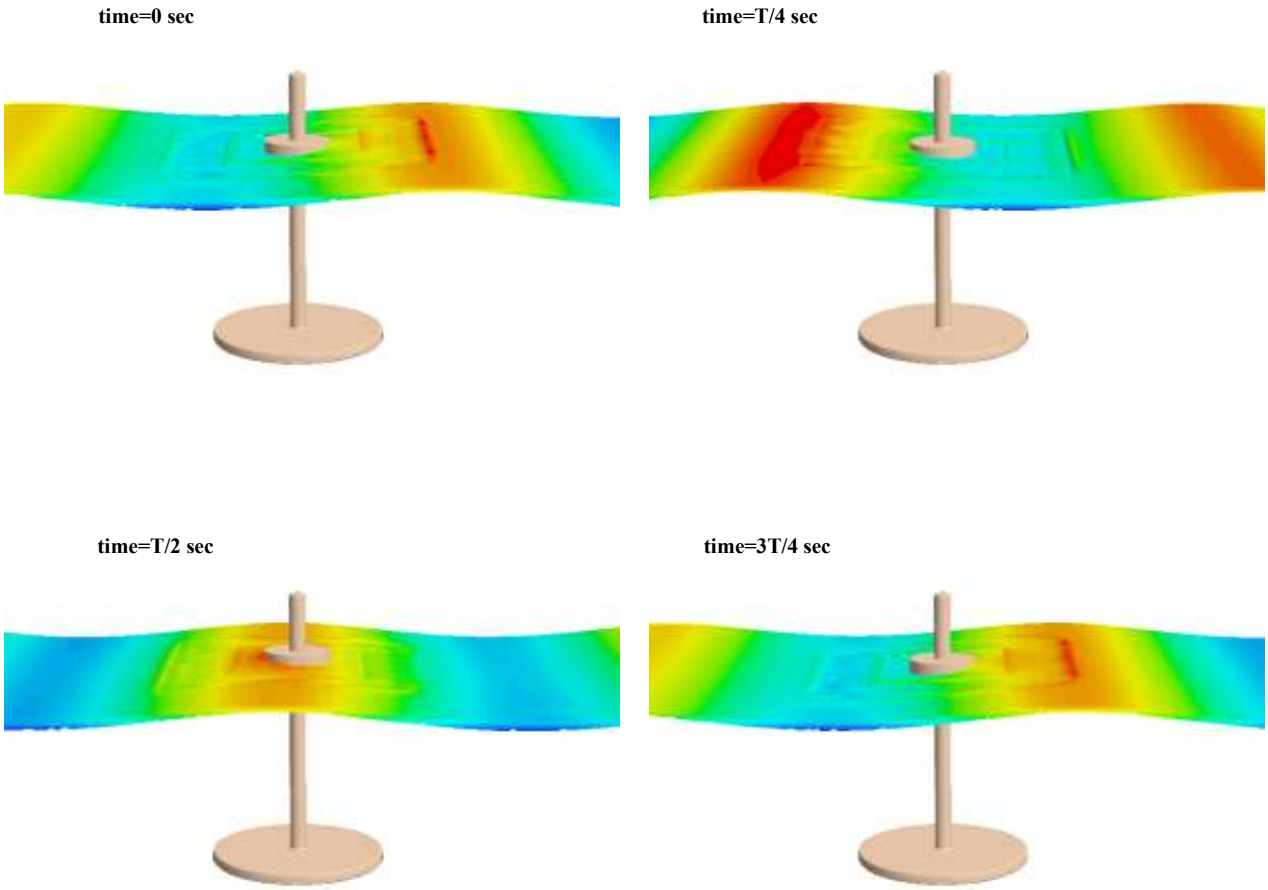

Figure 9: Free surface profiles at different time steps

4. Conclusions

This study presented a comprehensive CFD-based evaluation of a two-body floating point absorber (FPA) designed for deployment in the Gulf of Oman, with a particular focus on the influence of PTO damping and sea states on energy absorption. Using a high-fidelity URANS–VOF numerical framework with overset grids, the dynamic interaction between waves, floating bodies, and the PTO system was captured with high accuracy. Validation against experimental heave decay data confirmed that the numerical model reliably reproduces the hydrodynamic behavior of the device.

Based on the analysis of the absorbed power across varying sea states, wave height is the primary driver of power output, with absorbed energy increasing nearly quadratically with height, for instance, raising the wave height from 1.2 m to 2.0 m at the optimal period of 6 s resulted in more than a doubling of captured power. Simultaneously, the wave period determines the spectral tuning of the device. On the other hand, the performance bandwidth is relatively broad (5–7 s), which is beneficial for real-sea applications where periods vary. Below a threshold wave height of approximately 0.6 m, the absorbed power becomes negligible (<0.2 kW) regardless of period, defining a practical lower limit for viable energy extraction.

The results also show that PTO tuning plays a critical role in maximizing power capture, and that optimal performance is obtained when PTO parameters align the device's mechanical response with the dominant wave period of the environment. PTO damping was found to have a strong, frequency-dependent influence on performance. A clear optimal damping value of approximately 100 kNs/m emerged, corresponding to a wave period between 5-7 seconds, where the device exhibits near-resonant behavior. At this operating point, the absorbed power reaches its highest levels, consistent with the theoretical expectation that maximum power is achieved when mechanical damping is tuned to match hydrodynamic radiation damping.

Although the PTO optimization identified clear operational sweet spots, the absolute power levels obtained under realistic Gulf of Oman conditions remain relatively low. This limitation is attributed primarily to the weak wave energy climate of the region, which is enclosed by land and lacks significant long-period swells. Therefore, while the device design is hydrodynamically efficient, its deployment in the Gulf of Oman is unlikely to be economically viable. More energetic offshore locations or sites adjacent to open ocean swell would be better suited for exploiting

the full performance potential of this two-body FPA concept.

The study highlights the value of high-fidelity CFD simulations for capturing complex FSI dynamics and guiding PTO design. However, several opportunities exist for future work. These include extending the analysis to irregular and multidirectional waves, incorporating more realistic PTO control strategies, exploring the effects of extreme events, and evaluating additional WEC archetypes such as oscillating water columns or bottom-hinged flaps. The integration of optimization algorithms or machine-learning-based surrogate models could further accelerate the search for optimal PTO configurations. Such enhancements would provide deeper insight into device behavior across diverse sea states and support the development of more efficient and robust wave energy conversion systems.

5. References

Amiri, A., Panahi, R., & Radfar, S. (2016). Parametric study of two-body floating-point wave absorber. *Journal of marine science and application*, *15*, 41-49.

Beatty, S. J., Hall, M., Buckham, B. J., Wild, P., & Bocking, B. (2015). Experimental and numerical comparisons of self-reacting point absorber wave energy converters in regular waves. *Ocean Engineering*, *104*, 370-386.

Budar, K., & Falnes, J. (1975). A resonant point absorber of ocean-wave power. *Nature*, *256*(5517), 478-479.

Chen, H., Xu, Q., Zheng, X., Bennetts, L. G., Xie, B., Lin, Z., Lin, Z., & Li, Y. (2023). Viscous effects on the added mass and damping forces during free heave decay of a floating cylinder with a hemispherical bottom. *European Journal of Mechanics-B/Fluids*, *98*, 8-20.

Choi, J., & Yoon, S. B. (2009). Numerical simulations using momentum source wave-maker applied to RANS equation model. *Coastal Engineering*, *56*(10), 1043-1060.

Courant, R., Friedrichs, K., & Lewy, H. (1928). Über die partiellen Differenzengleichungen der mathematischen Physik. *Mathematische annalen*, *100*(1), 32-74.

Evans, D. (1976). A theory for wave-power absorption by oscillating bodies. *Journal of Fluid Mechanics*, *77*(1), 1-25.

Evans, D. (1981). Power from water waves. *Annual review of Fluid mechanics*, *13*, 157-187.

Falcão, A. F., & Henriques, J. C. (2015). Effect of non-ideal power take-off efficiency on performance of single-and two-body reactively controlled wave energy converters. *Journal of Ocean Engineering and Marine Energy*, *1*, 273-286.

Falnes, J. (1999). Wave-energy conversion through relative motion between two single-mode oscillating bodies.

Falnes, J. (2007). A review of wave-energy extraction. *Marine structures*, *20*(4), 185-201.

Ishaq, M., Chen, Z.-M., & Zhao, Q. (2023). Analysis of nonlinear water wave interaction solutions and energy exchange between different wave modes. *Physics of Fluids*, *35*(2).

Li, Y., & Yu, Y.-H. (2012). A synthesis of numerical methods for modeling wave energy converter-point absorbers. *Renewable and Sustainable Energy Reviews*, *16*(6), 4352-4364.

Liang, C., & Zuo, L. (2017). On the dynamics and design of a two-body wave energy converter. *Renewable energy*, *101*, 265-274.

Liu, Y., Zheng, S., Liang, H., & Cong, P. (2022). Wave interaction and energy absorption from arrays of complex-shaped point absorbers. *Physics of Fluids*, *34*(9).

Ma, Y., Zhang, A., Yang, L., Li, H., Zhai, Z., & Zhou, H. (2020). Motion simulation and performance analysis of two-body floating point absorber wave energy converter. *Renewable energy*, *157*, 353-367.

Mei, C. C. (1976). Power extraction from water waves. *Journal of Ship Research*, *20*(02), 63-66.

Newman, J. N. (1976). The interaction of stationary vessel with regular waves. International Proceedings of the 11th Symposium on Naval Hydrodynamics, ONR, 1976,

OPT. (2023). *Information about PB3 PowerBuoy wave energy device*. http://www.oceanpowertechnologies.com

Rhinefrank, K., Schacher, A., Prudell, J., Stillinger, C., Naviaux, D., Brekken, T., von Jouanne, A., Newborn, D., Yim, S., & Cox, D. (2010). High resolution wave tank testing of scaled wave energy devices. International Conference on Offshore Mechanics and Arctic Engineering,

Saket, A., & Etemad-Shahidi, A. (2012). Wave energy potential along the northern coasts of the Gulf of Oman, Iran. Renewable Energy, 40(1), 90-97.

Salter, S. H. (1974). Wave power. *Nature*, *249*(5459), 720-724.

Soleimani, K., Ketabdari, M. J., & Gharechae, A. (2023). Smoothed particle hydrodynamics study of a heaving point absorber in various waves using wave tank and calm-water models. *Physics of Fluids*, *35*(3).

Sricharan, V., & Chandrasekaran, S. (2021). Time-domain analysis of a bean-shaped multi-body floating wave energy converter with a hydraulic power take-off using WEC-Sim. *Energy*, *223*, 119985.

Stansby, P., Moreno, E. C., & Stallard, T. (2017). Large capacity multi-float configurations for the wave energy converter M4 using a time-domain linear diffraction model. *Applied Ocean Research*, *68*, 53-64.

Windt, C., Davidson, J., & Ringwood, J. V. (2021). Numerical analysis of the hydrodynamic scaling effects for the Wavestar wave energy converter. *Journal of Fluids and Structures*, *105*, 103328.

Xu, Q., Li, Y., Bennetts, L. G., Wang, S., Zhang, L., Xu, H., & Narasimalu, S. (2023). Parametric analysis of a two-body floating-point absorber wave energy converter. *Physics of Fluids*, *35*(9).

Yu, Y.-H., & Li, Y. (2013). Reynolds-Averaged Navier–Stokes simulation of the heave performance of a two-body floating-point absorber wave energy system. *Computers & Fluids*, *73*, 104-114.

Zheng, X., Chen, G., Cao, W., Xu, H., Zhao, R., Xu, Q., Kramer, M., Le Touzé, D., Borthwick, A. G., & Li, Y. (2021). On the energy conversion characteristics of a top-mounted pitching absorber by using smoothed particle hydrodynamics. *Energy Conversion and Management*, *250*, 114893.